Journal of Quantitative Spectroscopy & Radiative Transfer 109 (2008) 2195–2206

Journal of Quantitative Spectroscopy & Radiative Transfer

www.elsevier.com/locate/jqsrt

Light scattering in a finite multi-particle system

Evgenij Zubko[a,b], Yuriy Shkuratov[b,c], Michael Mishchenko[d], Gorden Videen[e,*]

[a]*Institute of Low Temperature Science, Hokkaido University Kita-ku North 19 West 8, Sapporo 060-0819, Japan*
[b]*Astronomical Institute of V.N. Karazin Kharkov National University, 35 Sumskaya St., Kharkov 61022, Ukraine*
[c]*Institute of Radio Astronomy of National Academy of Sciences of Ukraine, 4 Chervonopraporna Street, Kharkov 61002, Ukraine*
[d]*NASA Goddard Institute for Space Studies, 2880 Broadway, New York, NY 10025, USA*
[e]*Army Research Laboratory, AMSRL-CI-EM, 2800 Powder Mill Road, Adelphi, MD 20783, USA*

Received 30 November 2007; received in revised form 13 March 2008; accepted 14 March 2008

Abstract

We use the discrete dipole approximation (DDA) to perform electromagnetic scattering calculations of particles in a 3D volume. We adjust the spacing between the particles to change the volume densities of the scattering systems from approximately 10% to 100%. For very large volume densities, e.g. $>50\%$, it is difficult to assign unambiguously whether the system is composed of a single heterogeneous particle or of multiple particles. Our calculations demonstrate optical effects attributable to multiple scattering in systems having volume densities as high as $\sim 90\%$. This suggests that heterogeneities within naturally occurring particle systems can produce multiple-scattering effects. We also see evidence of very deep negative polarization branches (NPBs) ($\sim -6\%$) that may have implications in interpreting polarization phase curves of cometary circumnuclear halos.
Published by Elsevier Ltd.

Keywords: Negative polarization branch; Coherent backscattering; Multiple scattering

1. Introduction

Multiple scattering of electromagnetic waves in random media may result in two well-known backscattering phenomena: the intensity surge and the polarization opposition effect (POE). Both of these effects are the result of interference of reciprocal rays [1–46]. In the case of the intensity surge, constructive interference of reciprocal rays enhances intensities in the backscattering directions. In the case of polarization, constructive interference of reciprocal rays tends to enhance the TM component of the electromagnetic field preferentially, resulting in a polarization minimum in the near-backscattering direction. In the exact backscatter direction, the polarization state of the scattered light remains zero for random media illuminated by unpolarized light.

While the POE is the result of multiple scattering, the negative polarization branch (NPB) refers to a negative polarization minimum in the near-backscattering direction and generally is associated with single-particle scattering [47–68]. The NPB minimum typically occurs approximately within 10°–20° from the exact

*Corresponding author. Tel.: +1 301 394 1871; fax: +1 301 394 4797.
E-mail address: gvideen@arl.army.mil (G. Videen).

0022-4073/$ - see front matter Published by Elsevier Ltd.
doi:10.1016/j.jqsrt.2008.03.007

backscattering direction; whereas, the POE minimum typically occurs within a few degrees of the exact backscattering direction. The minima positions are an indication of spatial scales for the underlying phenomena and suggest that the NPB's mechanism acts on micron and submicron spatial scales; whereas, the POE mechanism acts on super-micron spatial scales. We characterize particle size using the size parameter $x = 2\pi r/\lambda$, where λ is the wavelength of incident wave and r is some characteristic size of the particle. In this study we use the radius of the circumscribing sphere and designate this size parameter as x_{cs}. We prefer to use the size parameter x_{cs} related to the radius of the circumscribing sphere because it gives information about the largest distance between two points in a scatterer. Another frequently used characterization is the radius of an equal-volume sphere, which we denote as x. We tend to see the NPB when x_{cs} is varied in the range from approximately 5% to $40 \pm 20\%$ [60]. For larger size parameters the negative polarization typically is the result of multiple scattering between distant scattering sites, and the mechanism describing this is that of the POE. While the POE minima tend to be asymmetric, those of the NPB appear more symmetric. Although the multiple-scattering mechanism for the POE is well established [1,3–5,9,15,16], the mechanism for the NPB is not. Researchers have attributed the phenomenon to internal [63,64] and near-field effects in single particles [33,61,62]. In the latter case, as it was shown in [57], neglecting the near-field component in dipole–dipole interaction has no dramatic influence on the NPB and the effect is produced primarily by the far-field component.

For some particle systems, like dipoles near surfaces, it can be demonstrated that a NPB is the result of interference of reciprocal rays [29], the same mechanism as the POE, but on a smaller spatial scale. In simulations of clusters of particles, it appears that the NPB of agglomerate particles also is a manifestation of the POE on very small spatial scales [40,56]. Zubko et al. [56] demonstrated that the NPB of clusters of particles depends primarily on the size of the particles making up the cluster, rather than the number of particles and overall size of the cluster, which is consistent with the interference mechanism.

Mishchenko et al. [40] tracked the evolution of various manifestations of the effect of coherent backscattering as the volume density was increased from essentially 0% to 24%. In this manuscript, we expand the study of Mishchenko et al. [40] to higher volume densities. By considering non-spherical particles, we are able to increase the volume density up to 1; i.e., until the separate particles coalesce to a single particle. This allows us to consider the evolution of the backscatter polarization from the region in which the multiple-scattering POE dominates to the region in which the NPB dominates.

2. Technique

We examine the transition of the scattering system from multiple particles until they coalesce to a single particle. To do this, we consider a single non-spherical particle and divide this particle into 30 randomly chosen segments. These segments are each of different shape and size. The size parameter of each equal-volume sphere x ranges from 0.9 to 3.5 with a mean value of about 2.5. Although all segments are comparable to the wavelength, the profile of linear polarization averaged over segments and their random orientations reveal only positive polarization over the entire range of phase angles. The polarization curve has a bell-like shape with maximum at a phase angle of approximately 70°. At $m = 1.5 + 0.01i$, its amplitude is 46%, while at $m = 1.5 + 0.1i$, it is 52%. We then explode the particle system, keeping the individual segments intact. This is done by moving the position of the center of mass of each segment by an amount proportional to its initial radius vector from the center of mass of the entire system: $\mathbf{R}_i = \beta \mathbf{R}_{io}$, where $\mathbf{R}_{io}$ is the initial radius vector of the center of mass of segment i with respect to the center of mass of the particle system, and $\mathbf{R}_i$ is the center of mass of segment i with respect to the center of mass of the particle system after the system has been expanded by a factor β. An example of the particle explosion process is shown in Fig. 1. The number shown in the upper right of each particle system indicates the expansion factor β.

As β increases, the system transitions from a single particle to multiple particles. It also incorporates more vacuous space within the particle system. One convenient way of quantifying the percentage of material in a porous object is through its volume density; however, for an irregularly shaped, finite, multi-particle system like that shown in Fig. 1, the definition of this quantity is ambiguous. In this manuscript we define the volume ratio as the volume of a sphere centered at the center of mass that circumscribes the particle at $\beta = 1$ divided by the volume of a sphere centered at the center of mass that circumscribes the particle system at β. In this

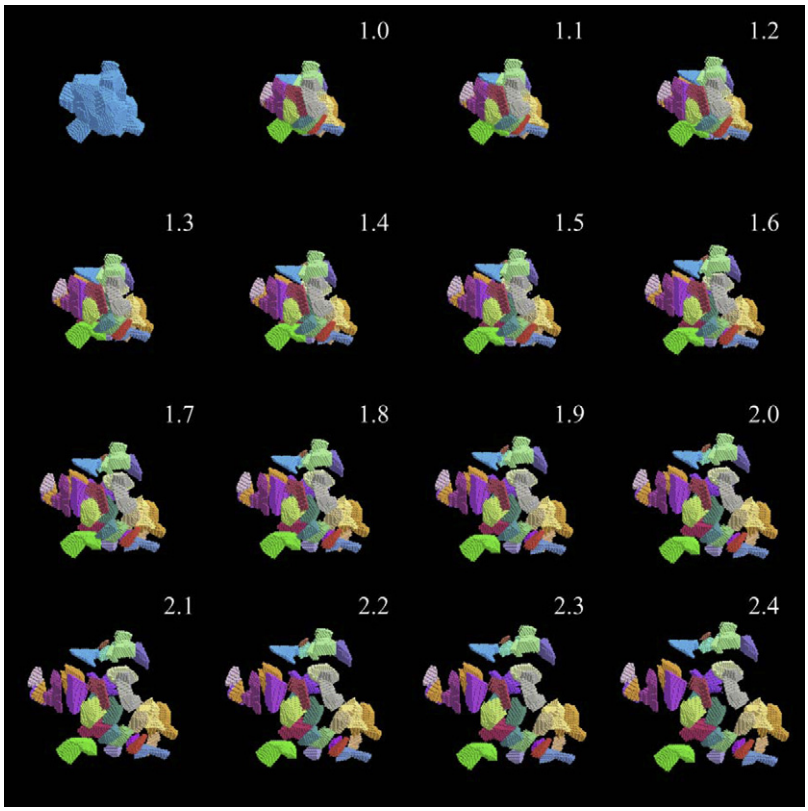

Fig. 1. Images of a particle exploding into 30 fragments at various expansion factors β.

Table 1
Volume density calculated from $V(1)/V(\beta)$, where $V(\beta)$ is the volume of the circumscribing sphere centered at the center of mass of the particle having expansion factor β

β	$V(1)/V(\beta)$
1	1
1.1	0.897258
1.2	0.71949
1.3	0.544912
1.4	0.465089
1.5	0.387348
1.6	0.308728
1.7	0.262336
1.8	0.221133
1.9	0.191719
2	0.166289
2.1	0.140637
2.2	0.126803
2.3	0.112282
2.4	0.0963702

way, the volume ratio of the single-particle system ($\beta = 1$) is 1. Table 1 presents the volume densities calculated from the particle system realizations of Fig. 1.

We generate the initial unexploded particle using the algorithm to generate agglomerated debris particles described in Zubko et al. [59]. According to the algorithm, we generate a 3D space in computer memory and

fill it with a cubic lattice. We introduce a sphere with a radius of 32 cells, which spans the lattice. The 137,376 cells located inside the sphere are used in the generation procedure. These cells comprise the initial matrix. Among cells located on the surface of the initial matrix we choose 100 at random, which are marked as seeds of empty space. Interior to the surface we choose an additional 20 random seeds of empty space and 21 of material. Then step-by-step each cell within the initial matrix is designated with the property of the nearest seed cell, either material or empty space. The resulting particle appears as an irregular, agglomerated particle. On average, these particles occupy about 26% of the initial matrix volume. Images of sample particles generated with the given procedure, as well as the light scattering properties of agglomerated debris particles under various conditions, can be found in [59].

The algorithm described above typically generates particles having a very open structure whose constituent parts are separated by empty space. This feature is not desirable for the present study because we are interested in particles having more or less compact structure; however, such particles appear with a probability of 10%. One particle having compact structure is shown in the upper left panel of Fig. 1. This particle consists of 43,748 dipoles, which correspond to approximately 32% of the initial matrix volume.

The scattering properties of the system are calculated using the discrete dipole approximation (DDA) [69–72]. The algorithm we use has been tested and described previously [54–60,63,72]. In the DDA approach, the particle system is represented by an array of dipoles. In our simulations we use a $64 \times 64 \times 64$ grid. Each dipole is assigned the optical properties of the local material of the system it is representing. The dipole moment at each location is the result of the excitation of the incident electromagnetic field and the scattered electromagnetic fields from all the other dipoles. The scattered field is the superposition of the scattered fields from all the dipoles.

While the primary advantage of using the DDA over the T-matrix method is that the scattering particle is discretized and can have any morphology, one disadvantage is that no algorithm exists for obtaining orientation-averaged scattering properties rapidly. Obtaining such properties is extremely computationally expensive. In order to accelerate the DDA computations we split the averaging process into two sub-processes: averaging over orientations of the incident beam and averaging over different scattering planes. Each new orientation in the former case requires recalculating the electric fields induced on the array of dipoles. This procedure requires the bulk of the CPU time. Once a set of the induced fields has been received we compute the fields scattered in the far zone. Because this process requires a negligible amount of time, we repeat our computations in 100 scattering planes evenly distributed around the wavevector of the incident field and average these results.

The number of orientations of the incoming beam used in the averaging process depends on the particular sample, as some particles have greater variance in their backscattering than others. The average number of orientations used in our calculations is approximately 700. Typically, this number varied between 450 and 1000, with the maximum number of orientations being 1500. To test for convergence, we perform averaging in two sub-processes, each based on half of the scattering planes used in each sample (i.e., on 50 scattering planes). We compare results of both sub-processes to the results obtained when averaging over 100 scattering planes. As a quantitative indicator of the averaging, we use the standard deviation of the linear degree of polarization obtained with 100 and 50 scattering planes. This deviation is phase-angle dependent and was limited to 1%. For the backscattering regime ($\alpha < 30^\circ$), this value is typically less.

3. Results

Fig. 2 shows maps of the electromagnetic scattering intensities (left) and polarizations (right) of the irregularly shaped particles of Fig. 1 as functions of the expansion factor and phase angle. The top figures are calculated for $m = 1.5 + 0.01i$, while the bottom figures are calculated for $m = 1.5 + 0.1i$. For both sets of particles, we see that for small expansion factors the polarization levels tend to remain relatively low, $<10\%$. While the values for this single-particle case tend to be positive throughout most of the angular range, this is not the case with all particles we examined. As the expansion factor increases, the system is transformed from an irregularly shaped particle system to a dense cloud of irregularly shaped, small particles. During this transformation, the central scattering intensity peak increases in both height and breadth. This is consistent with the interference mechanism. In addition, the polarization increases, especially at midrange scattering

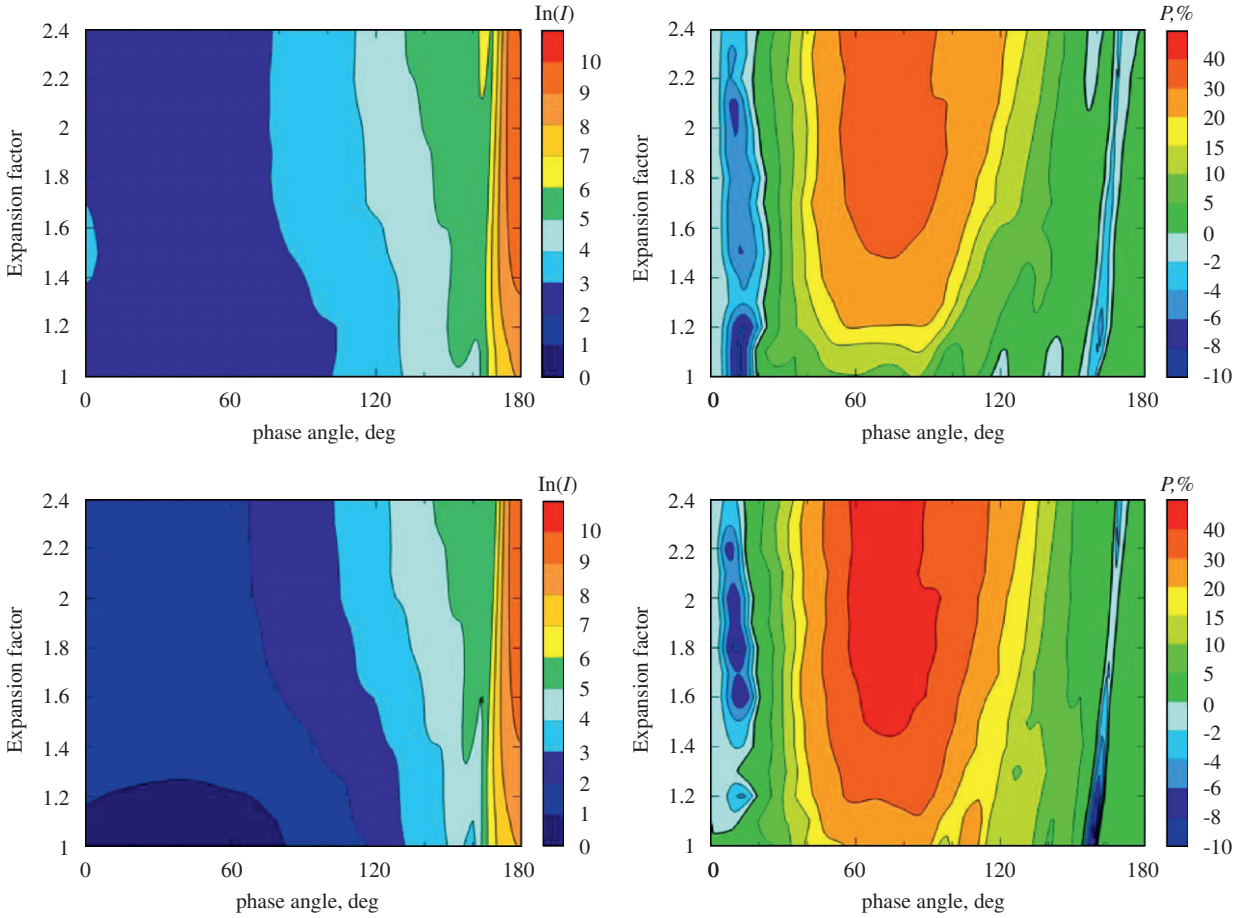

Fig. 2. Maps of intensity I (left column) and degree of linear polarization P (right column) as a function of phase angle α and the expansion factor β of the model particle of Fig. 1 at size parameter of $x_{cs} = 12$: the case of $m = 1.5 + 0.01i$ on top and $m = 1.5 + 0.1i$ on bottom.

angles near 90°, to levels greater than 30%. This mid-range increase in positive polarization is reminiscent of the scattering from single, small particles. It also resembles the polarization response from terrestrial and cometary dust particles [30–32,49–51,65–68,73,74]. We note that the level of polarization is greater for the more absorbing particles that are able to suppress the multiple-scattering components of the fields.

One interesting feature is the negative polarization trench seen in Fig. 2 at phase angles of approximately 160° (scattering angles of approximately 20°). This trench shifts to smaller scattering angles as the expansion factor increases, suggesting an interference mechanism. Its origin is in fact the first diffraction minimum. The forward scattering is dominated by diffraction and the TE intensities tend to be larger than the TM intensities in this region, which leads to positive polarization values. However, at the minima locations the diffraction minima tend to be deeper for the TE mode than for the TM mode, resulting in negative polarization. While these minima are a prominent feature of the polarization mappings, they are a minor feature of the intensity mappings. For a wide polydispersion of particles, this feature would not be visible.

The focus of this study is polarization backscattering phenomena. It is well established that the POE is the result of multiple scattering by particulate media. What is not established is how densely packed a medium can be to manifest this phenomenon. Because of the nature of the spherical particles used in the previous study [40] and required randomness in particle orientation, it is difficult to achieve significantly larger packing densities. By commencing our study with a solid particle and dividing it into segments of small particles, we can consider packing densities as high as 100%; i.e., until the particles coalesce to a single particle. The POE is clearly visible as a trough located at approximately 10° in both polarization mappings of Fig. 2. This trough extends

all the way to an expansion factor of 1.0 (to the single particle limit) for the $m = 1.5 + 0.01i$ case and to an expansion factor less than 1.1, corresponding to packing densities greater than 90%, for the $m = 1.5 + 0.1i$ case.

One challenge of considering larger packing densities is consideration of the single-particle polarization. Single particles may form either an NPB or positive polarization branch (PPB) in the near-backscatter direction when the scattering signal is averaged over particle orientations. In our simulations, we have found that PPBs are observed much more frequently in spheres and spheroids than in irregularly shaped particles, but are more common in the latter class when particle absorption is increased [59,63]. The mappings of Fig. 2 show the orientation-averaged mappings of two systems having identical morphologies, but different refractive index m. For $m = 1.5 + 0.01i$, shown in the top, an NPB is visible for an expansion factor close to 1.0, while for $m = 1.5 + 0.1i$, shown in the bottom, a PPB is visible for an expansion factor close to 1.0. What is interesting about this bottom mapping is that a negative branch of polarization becomes established near 1.1. This negative branch retains some of the same characteristics of both branches as the expansion factor β increases, like the minimum near $\beta = 1.3$ and the decrease in polarization for large β approaching 2.4. Fig. 3 shows a plot of the magnitude of the polarization minimum $P_{\min}$ as a function of the expansion factor for the two systems shown in Fig. 2. Once the minimum becomes well established for the more absorbing case, the dependence of the amplitude with growing expansion factor is similar in both systems. The primary difference between the two particle systems is the higher level of negative polarization in the less absorbing system. This common behavior suggests a common mechanism for both systems, the same multiple-scattering interference mechanism that results in the POE. When the expansion factor approaches $\beta = 1$, this mechanism competes with the single-particle mechanism that produces the NPB; however, it appears that the POE is present even for small $\beta \sim 1.1$.

Accompanying the POE is the backscattering intensity surge that is also the result of the coherent backscattering mechanism. The apparent absence of this surge in Fig. 2 is due to the logarithmic plot. Fig. 4 shows the scattered intensities in the backscatter region plotted on a linear plot, normalized at phase angle $\alpha = 0°$. An intensity surge is clearly visible in these plots over the entire range of expansion factors.

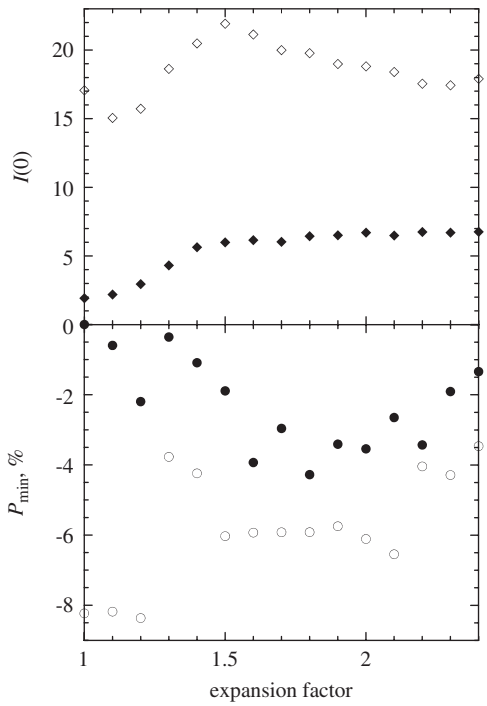

Fig. 3. Intensity at zero phase angle (top) and depth of the negative polarization (bottom) as a function of expansion factor β taken from the data of Fig. 2. Open symbols correspond to the case of $m = 1.5 + 0.01i$, whereas filled symbols correspond to the case of $m = 1.5 + 0.1i$.

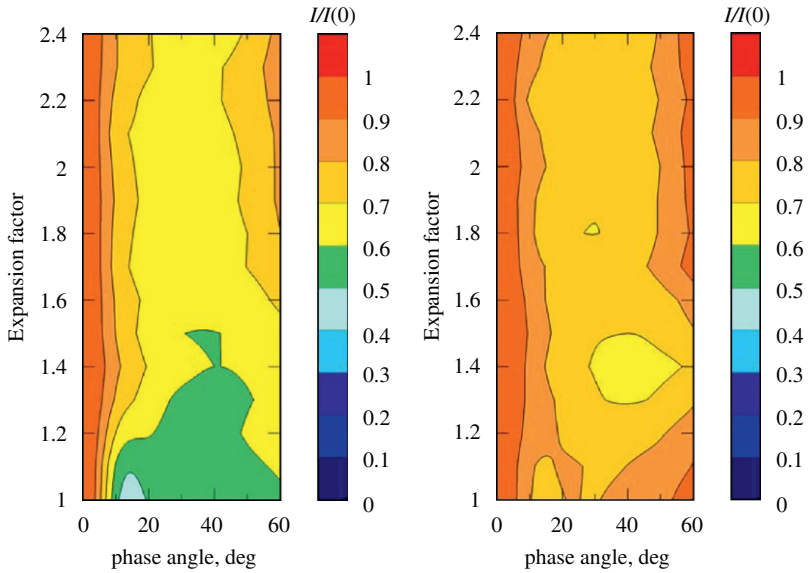

Fig. 4. Intensity of light scattering near backscattering (linear scale). Maps are normalized at phase angle $\alpha = 0°$. Left panel corresponds to $m = 1.5 + 0.01i$ and right panel to $m = 1.5 + 0.1i$.

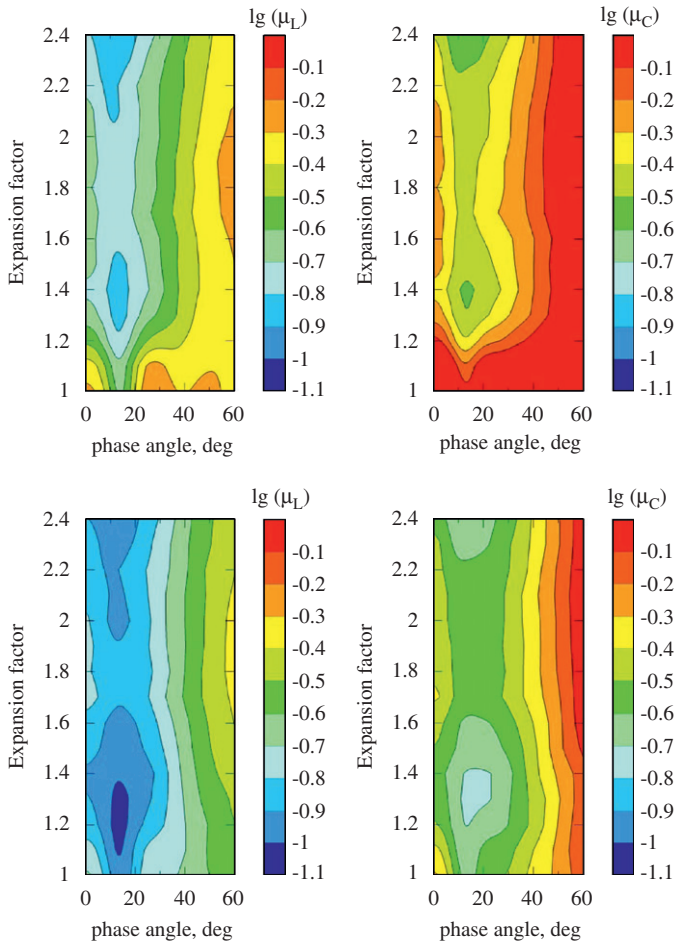

Fig. 5. Ratios μ_L and μ_C near backscattering. Upper row corresponds to $m = 1.5 + 0.01i$ and bottom to $m = 1.5 + 0.1i$.

One other consideration for the coherent-backscattering mechanism is the polarization ratios. The linear polarization ratio μ_L is defined as the ratio of the cross-polarized to co-polarized scattered intensity

$$\mu_L(\alpha) = \frac{S_{11}(\alpha) - S_{22}(\alpha)}{S_{11}(\alpha) + 2S_{12}(\alpha) + S_{22}(\alpha)}, \tag{1}$$

where the $S_{ij}(\alpha)$ are the light scattering Mueller matrix elements at phase angle α. The circular polarization ratio μ_C is defined as the ratio of the same helicity to the opposite helicity scattered intensity

$$\mu_C(\alpha) = \frac{S_{11}(\alpha) + S_{44}(\alpha)}{S_{11}(\alpha) - S_{44}(\alpha)}. \tag{2}$$

Both these quantities approach zero in the backscattering as the amount of multiple scattering approaches zero and the particles are spherical. We plot these components in Fig. 5. We observe that the overall magnitude of these ratios is significantly smaller for the system composed of the more absorbing particles (bottom panels). Absorption tends to reduce preferentially the multiply scattered component. These results also demonstrate local maxima in both μ_L and μ_C in the backscatter direction. The widths of these peaks are much narrower than features that could be produced from any of the individual small particles, so they must be the result of multiple scattering. Its presence is consistent with the coherent backscattering mechanism that enhances multiply scattered components in the backscatter region. Finally, we note that the circular polarization ratio is greater than the linear polarization ratio. This is also consistent with results of computations of the coherent backscattering for plane-parallel layers of spherical particles [75].

4. Discussion

When considering multiple scattering, or scattering by multiple particles located in a volume, there are two limits on volume density to consider. First, how far apart must the particles be for the single-scattering approximation to be considered valid? Second, how close must particles be before we can consider the system to comprise a single particle? In a previous study [41], the low-density limit was considered. For many intensity-related observables like extinction, the separation distances between the particles must be much greater than either the wavelength or particle dimensions. However, for other observables, like certain polarization features, these criteria can be relaxed substantially.

The high-density limit was also considered in a study of light scattering from a volume filled with small, randomly located spheres [40]. The present manuscript reports on an expansion of this study with the difference that the particles are no longer spherical and can be packed together to form a single particle system. These changes allow us to consider much higher volume densities, even up to 100%. As a particle system approaches the single-particle limit where $\beta \to 1.0$, it may become difficult to distinguish the multiple-scattering POE from the single-scattering NPB. To try to distinguish these effects, we consider single-particle systems that displayed NPBs and others that displayed a PPB. We present maps of the scattering properties of examples of each of these systems as they exploded into fragments. We find that both systems appear to display a POE for expansion factors as low as ~1.1 (corresponding to a volume fraction of ~90%), and these negative polarizations are retained for expansion factors to 2.4 (corresponding to a volume fraction of ~10%), the limit of our calculations in this study. Examination of backscattering intensity maps reveals a surge whose dimensions are comparable to those of the polarization features that we consider. In addition, plots of the linear and circular polarization ratios suggest an enhancement of the multiply scattered components in the backscattering region that is consistent with the coherent backscattering mechanism. While these tests do not prove that the backscattering phenomena from such dense particle systems are the result of coherent backscattering, the results are consistent with the mechanism, meaning the resulting polarization features for such particles are a manifestation of the POE.

Observing the POE at such large packing densities has implications in our consideration of particulate scattering. Naturally occurring particles are rarely homogeneous and typically contain heterogeneities on the submicron scale. Fig. 6, for instance, shows a mass spectrometer image of a Saharan dust grain along with a photomicrograph of another Saharan dust grain. Fig. 6a shows a significant percentage of submicron-size regions of concentrated calcium and aluminum within a silicate matrix. Based on astrophysical observations,

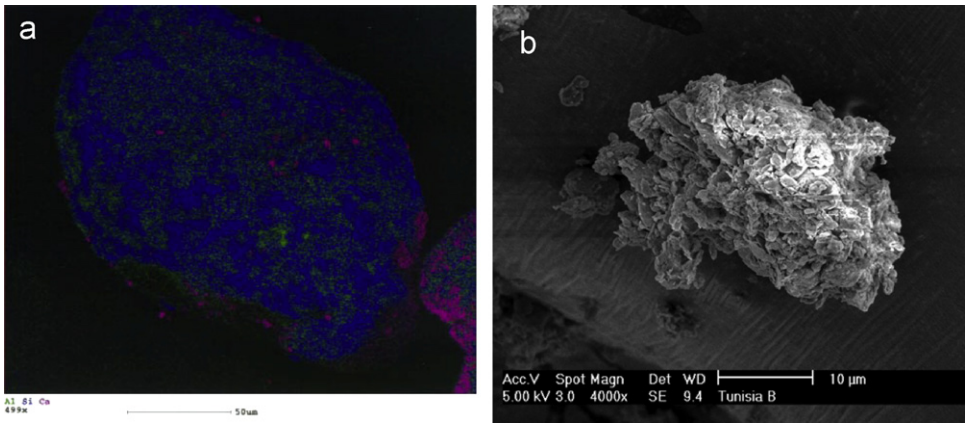

Fig. 6. (a) Mass spectrometer image of a Saharan dust grain showing elemental composition: Al, green; Si, blue; Ca, pink; and (b) Saharan dust agglomerate (photomicrograph taken by Timo Nousiainen).

cosmic dust grains are portrayed as heterogeneous systems composed of submicron particulates of ice, silicates, carbon, organic material, etc. The photomicrograph (Fig. 6b) shows one of many agglomerate particles that have a significant amount of air and a resulting volume density that is significantly less than 100%. Our simulations suggest that the heterogeneities and voids contained within such naturally occurring particles could result in coherent backscattering and that this mechanism may be responsible for the ubiquitous NPB.

Finally, we would like to emphasize one important outcome of this work for cometary physics. Imaging polarimetry of comets shows the presence of a bright cloud around the nucleus called a cirumnuclear halo, whose radii typically are on the order of 2000 km that produce systematically low linear polarizations [73,74]. In the range of small phase angles, a circumnuclear halo reveals a pronounced NPB whose depth is approximately −6% [73,74]. Such a deep NPB has been interpreted as evidence that these haloes must be produced by dust particles having a compact structure [74]. That conclusion is consistent with numerical simulation results of light scattering by porous ballistic particle–cluster aggregates (BPCA) and an extremely porous ballistic cluster–cluster aggregate (BCCA) [65–68]. As demonstrated in these manuscripts, both BCCAs and BPCAs consisting of Rayleigh-size particles having typical refractive indices of silicates reveal very shallow NPBs of about −0.5%. The NPB depth increases with real part of refractive index and size parameter of constituent grains x_{mon} to approximately −6% in the case of $\mathrm{Re}(m) = 2$ and $x_{\mathrm{mon}} = 1.26$ [68]. Organic material is the only significant cometary component having such large real refractive index [76,77], but it is accompanied by a noticeably high imaginary part, which effectively decreases the NPB depth [68]. In simulations of silicates of $\mathrm{Re}(m) = 1.6$, both fluffy structures BPCA and BCCA do not produce deep NPBs at size parameters of constituent spheres up to 1.26 [68]. Further increasing the size of the constituent spheres produces linear-polarization curves having strong oscillations resembling those of the single sphere [65].

Our numerical simulations do not produce such angular resonances, since our systems are composed of irregularly shaped fragments. They produce a featureless bell-shaped curve of linear polarization despite the relatively large size parameter of about 2.5. Our simulations lead to another explanation of deep NPB produced by circumnuclear halo. As one can see from Fig. 3, the exploding particle does not reveal a rapid decrease in the NPB amplitude and, in the case of weak absorption, even the sparse system at $\beta = 2$ (corresponding to a volume density $\rho = 0.166$) shows a deep NPB with an amplitude of −6.1%. The explanation of this behavior is rather simple: the deep NPB of the fluffy agglomerate results from the size of the constituent grains, which in our simulations have a size parameter of $x = 2.5$. An essential feature of such grains is that their scattering cross-section is visibly larger than the geometrical one, enhancing the multiple-scattering component that contributes to the NPB.

Thus, a deep NPB is not sufficient to distinguish compact from fluffy particles, since fluffy particles composed of small, but non-Rayleigh-sized, constituents can also produce deep NPBs. One distinguishing quantity is the ratio of $P_{\max}$ to $|P_{\min}|$. If this ratio is low it suggests a compact structure of dust particles

(see Fig. 2); whereas, if it is high other options are available: fluffy aggregates composed of strongly scattering grains, compact particles consisting of optically soft material, e.g., ice [59]. In addition, our simulations suggest that compact particles containing small, but non-Rayleigh-sized, heterogeneities may also produce such effects.

Acknowledgment

EZ is thankful for the financial support to the Grants-in-Aid program of Japan Society for the Promotion of Science.

References

[1] Shkuratov YuG. On the origin of the opposition effect and negative polarization for cosmic bodies with solid surface. Astron Cir (Sternberg State Astron Inst, Moscow) 1985;14:3–6.
[2] Shkuratov YuG. The diffraction mechanism of opposition effect of surface with complex structure. Kinematika i Fisika Nebesnykh Tel 1988;4:33–9.
[3] Shkuratov YuG. Interference mechanism of opposition spike and negative polarization of atmosphereless planetary bodies. Bull Am Astron Soc 1989;21:989.
[4] Shkuratov YuG. A new mechanism of the negative polarization of light scattered by the surfaces of atmosphereless celestial bodies. Astron Vestn 1989;23:176–80.
[5] Muinonen K. Electromagnetic scattering by two interacting dipoles. Proc 1989 URSI EM Theory Symp 1989:428–30.
[6] Muinonen KO, Sihvola AH, Lindell IV, Lumme KA. Scattering by a small object close to an interface. I. Study of backscattering. J Opt Soc Am A 1991;8:477–82.
[7] Mishchenko MI. Polarization effects in weak localization of light: calculation of the copolarized and depolarized backscattering enhancement factors. Phys Rev B 1991;44:12,597–600.
[8] Mishchenko MI. Enhanced backscattering of polarized light from discrete random media. J Opt Soc Am A 1992;9:978–82.
[9] Mishchenko MI. On the nature of the polarization opposition effect exhibited by Saturn's rings. Astrophys J 1993;411:351–61.
[10] Muinonen K. Coherent backscattering by solar system dust particles. In: Milani A, Di Martino M, Cellino A, editors. Asteroids, comets and meteors. Dordrecht: Kluwer; 1994. p. 271–96.
[11] Mishchenko MI. Diffuse and coherent backscattering by discrete random media. I. Radar reflectivity, polarization ratios, and enhancement factors for a half-space of polydisperse, nonabsorbing and absorbing spherical particles. JQSRT 1996;56:673–702.
[12] Rosenbush VK, Avramchuk VV, Rosenbush AE, Mishchenko MI. Polarization properties of the Galilean satellites of Jupiter: observations and preliminary analysis. Astrophys J 1997;487:402–14.
[13] Shkuratov Y, Kreslavsky M, Ovcharenko A, Stankevich D, Zubko E, Pieters C, et al. Opposition effect from Clementine data and mechanisms of backscatter. Icarus 1999;141:132–55.
[14] Tishkovets VP, Shkuratov YG, Litvinov PV. Comparison of collective effects at scattering by randomly oriented clusters of spherical particles. JQSRT 1999;61:767–73.
[15] Mishchenko MI, Luck J-M, Nieuwenhuizen TM. Full angular profile of the coherent polarization opposition effect. J Opt Soc Am A 2000;17:888–91.
[16] Shkuratov Yu, Ovcharenko A, Zubko E, Miloslavskaya O, Muinonen K, Piironen J, et al. The opposition effect and negative polarization of structural analogs of planetary regoliths. Icarus 2002;159:396–416.
[17] Videen G. Polarization opposition effect and second-order ray-tracing. Appl Opt 2002;41:5115–21.
[18] Tishkovets VP, Litvinov PV, Lyubchenko MV. Coherent opposition effects for semi-infinite discrete random medium in the double-scattering approximation. JQSRT 2002;72:803–11.
[19] Rosenbush V, Kiselev N, Avramchuk V, Mishchenko M. Photometric and polarimetric opposition phenomena exhibited by solar system bodies. In: Videen G, Kocifaj M, editors. Optics of cosmic dust. Dordrecht: Kluwer; 2002. p. 191–224.
[20] Shkuratov YG, Ovcharenko AV. Experimental modeling of opposition effect and negative polarization of regolith-like surfaces. In: Videen G, Kocifaj M, editors. Optics of cosmic dust. Dordrecht: Kluwer; 2002. p. 225–38.
[21] Mishchenko M, Tishkovets V, Litvinov P. Exact results of the vector theory of coherent backscattering from discrete random media: an overview. In: Videen G, Kocifaj M, editors. Optics of cosmic dust. Dordrecht: Kluwer; 2002. p. 239–60.
[22] Muinonen K, Videen G, Zubko E, Shkuratov Yu. Numerical techniques for coherent backscattering by random media. In: Videen G, Kocifaj M, editors. Optics of cosmic dust. Dordrecht: Kluwer; 2002. p. 261–82.
[23] Litvinov PV, Tishkovets VP, Muinonen K, Videen G. Coherent opposition effect for discrete random media. In: van Tiggelen B, Skipetrov SE, editors. Wave scattering in complex media. Dordrecht: Kluwer; 2003. p. 567–81.
[24] Videen G. Polarization opposition effect and second-order ray-tracing: cloud of dipoles. JQSRT 2003;79–80:1103–9.
[25] Videen G, Muinonen K, Lumme K. Coherence, power laws, and the negative polarization surge. Appl Opt 2003;42:3647–52.
[26] Tishkovets VP, Mishchenko MI. Coherent backscattering of light by a layer of discrete random medium. JQSRT 2004;86:161–80.
[27] Muinonen K. Coherent backscattering of light by complex random media of spherical scatterers: numerical solution. Waves Random Media 2004;14:365–88.

[28] Shkuratov Yu, Videen G, Kreslavsky M, Belskaya I, Kaydash V, Ovcharenko A, et al. Scattering properties of planetary regoliths near opposition. In: Videen G, Yatskiv Y, Mishchenko M, editors. Photopolarimetry in remote sensing. Dordrecht: Kluwer; 2004. p. 191–208.
[29] Videen G, Muinonen K. Backscattering from particles near planar surfaces. In: Videen G, Yatskiv Y, Mishchenko M, editors. Photopolarimetry in remote sensing. Dordrecht: Kluwer; 2004. p. 209–20.
[30] Levasseur-Regourd AC. Polarimetry of dust in the solar system: remote observations in-situ measurements and experimental simulations. In: Videen G, Yatskiv Y, Mishchenko M, editors. Photopolarimetry in remote sensing. Dordrecht: Kluwer; 2004. p. 393–410.
[31] Kiselev N, Rosenbush V. Polarimetry of comets: progress and problems. In: Videen G, Yatskiv Y, Mishchenko M, editors. Photopolarimetry in remote sensing. Dordrecht: Kluwer; 2004. p. 411–30.
[32] Kolokolova L, Kimura H, Mann I. Characterization of dust particles using photopolarimetric data: example of cometary dust. In: Videen G, Yatskiv Y, Mishchenko M, editors. Photopolarimetry in remote sensing. Dordrecht: Kluwer; 2004. p. 431–54.
[33] Tishkovets V, Litvinov P, Petrova E, Jockers K, Mishchenko M. Backscattering effects for discrete random media: theoretical results. In: Videen G, Yatskiv Y, Mishchenko M, editors. Photopolarimetry in remote sensing. Dordrecht: Kluwer; 2004. p. 221–42.
[34] Videen G, Wetmore A, Petre M, Shkuratov Y. Analytic description of enhanced backscattering and negative polarization from a cloud of dipoles. JQSRT 2006;100:406–14.
[35] Mishchenko MI, Rosenbush VK, Kiselev NN. Weak localization of electromagnetic waves and opposition phenomena exhibited by high-albedo atmosphereless solar system objects. Appl Opt 2006;45:4459–63.
[36] Bondarenko S, Ovcharenko A, Shkuratov Y, Videen G, Eversole J, Hart M. Light backscatter by surfaces composed of small spherical particles. Appl Opt 2006;45:3871–7.
[37] Ovcharenko AA, Bondarenko SY, Zubko ES, Shkuratov YG, Videen G, Nelson RM, et al. Particle size effect on the opposition spike and negative polarization. JQSRT 2006;101:394–403.
[38] Ovcharenko A, Bondarenko S, Shkuratov Yu, Scotto C, Hart M, Eversole J, et al. Backscatter effects of surfaces composed of dry biological particles. JQSRT 2006;101:462–70.
[39] Mishchenko MI, Liu L. Weak localization of electromagnetic waves by densely packed many-particle groups: exact 3D results. JQSRT 2007;106:616–21.
[40] Mishchenko MI, Liu L, Mackowski DW, Cairns B, Videen G. Multiple scattering by random particulate media: exact 3D results. Opt Express 2007;15:2822–36.
[41] Mishchenko MI, Liu L, Videen G. Conditions of applicability of the single-scattering approximation. Opt Express 2007;15:7522–7.
[42] Stankevich D, Istomina L, Shkuratov Y, Videen G. Electromagnetic phase differences in the coherent backscattering enhancement mechanism for random media consisting of large nontransparent spheres. Appl Opt 2007;46:1562–7.
[43] Psarev V, Ovcharenko A, Shkuratov Yu, Belskaya I, Videen G. Photometry of particulate surfaces at extremely small phase angles. JQSRT 2007;106:455–63.
[44] Litvinov P, Tishkovets V, Ziegler K. Coherent backscattering effects for discrete random media: numerical and theoretical results. JQSRT 2007;103:131–45.
[45] Shkuratov Yu, Bondarenko S, Kaydash V, Videen G, Muñoz O, Volten H. Photometry and polarimetry of particulate surfaces and aerosol particles over a wide range of phase angles. JQSRT 2007;106:487–508.
[46] Stankevich D, Istomina L, Shkuratov Yu, Videen G. The scattering matrix of random media consisting of large opaque spheres calculated using ray tracing and accounting for coherent backscattering enhancement. JQSRT 2007;106:509–19.
[47] Lumme K, Rahola J. Light scattering by porous dust particles in the discrete-dipole approximation. Astrophys J 1994;425:653–67.
[48] Lumme K, Rahola J, Hovenier JW. Light scattering by dense clusters of spheres. Icarus 1997;126:455–69.
[49] Muñoz O, Volten H, de Haan J, Vassen W, Hovenier J. Experimental determination of scattering matrices of olivine and Allende meteorite particles. Astron Astrophys 2000;360:777–88.
[50] Volten H, Muñoz O, Rol E, de Haan J, Vassen W, Hovenier J, et al. Scattering matrices of mineral aerosol particles at 441.6 nm and 632.8 nm. J Geophys Res 2001;106:17,375–401.
[51] Muñoz O, Volten H, Hovenier JW. Experimental light scattering matrices relevant to cosmic dust. In: Videen G, Kocifaj M, editors. Optics of cosmic dust. Dordrecht: Kluwer; 2002. p. 57–70.
[52] Muñoz O, Volten H, Hovenier JW, Min M, Shkuratov YuG, Jalava JP, et al. Experimental and computational study of light scattering by irregular particles with extreme refractive indices: hematite and rutile. Astron Astrophys 2006;446:525–35.
[53] Vilaplana R, Moreno F, Molina A. Computations of the single scattering properties of an ensemble of compact and inhomogeneous rectangular prisms: implications for cometary dust. JQSRT 2004;88:219–31.
[54] Zubko ES, Kreslavskii MA, Shkuratov YuG. The role of scatterers comparable to the wavelength in forming negative polarization of light. Solar Syst Res 1999;33:296–301.
[55] Zubko ES, Shkuratov YuG, Hart M, Eversole J, Videen G. Backscattering and negative polarization of agglomerate particles. Opt Lett 2003;28:1504–6.
[56] Zubko E, Shkuratov Yu, Hart M, Eversole J, Videen G. Backscattering of agglomerate particles. JQSRT 2004;88:163–71.
[57] Zubko E, Shkuratov Yu, Videen G. A discrete-dipole analysis of backscatter features of agglomerated debris particles comparable in size with wavelength. JQSRT 2006;100:483–8.
[58] Zubko E, Shkuratov Y, Muinonen K, Videen G. Collective effects by agglomerated debris particles in the backscatter. JQSRT 2006;100:489–95.
[59] Zubko E, Shkuratov Yu, Kiselev NN, Videen G. DDA simulations of light scattering by small irregular particles with various structure. JQSRT 2006;101:416–34.

[60] Zubko E, Shkuratov Yu, Muinonen K, Yamamoto T, Videen G. Light scattering by debris irregular particles with sizes a few times larger than wavelength, ApJ, 2008, submitted for publication.
[61] Tishkovets VP, Petrova EV, Jockers K. Optical properties of aggregate particles comparable in size to the wavelength. JQSRT 2004;86:241–65.
[62] Petrova EV, Tishkovets VP, Jockers K. Polarization of light scattered by solar system bodies and the aggregate model of dust particles. Solar Syst Res 2004;38:309–24.
[63] Muinonen K, Zubko E, Tyynelä J, Shkuratov YG, Videen G. Light scattering by Gaussian random particles with discrete-dipole approximation. JQSRT 2007;106:360–77.
[64] Tyynelä J, Zubko E, Videen G, Muinonen K. Interrelating angular scattering characteristics to internal electric fields for wavelength-scale spherical particles. JQSRT 2007;106:520–34.
[65] Kimura H. Light-scattering properties of fractal aggregates: numerical calculations by a superposition technique and the discrete-dipole approximation. JQSRT 2001;70:581–94.
[66] Kimura H, Kolokolova L, Mann I. Optical properties of cometary dust. Constraints from numerical studies on light scattering by aggregate particles. Astron Astrophys 2003;407:L5–8.
[67] Kimura H, Mann I. Light scattering by large clusters of dipoles as an analog for cometary dust aggregates. JQSRT 2004;89:155–64.
[68] Kimura H, Kolokolova L, Mann I. Light scattering by cometary dust numerically simulated with aggregate particles consisting of identical spheres. Astron Astrophys 2006;449:1243–54.
[69] Purcell EM, Pennypacker CR. Scattering and absorption of light by nonspherical dielectric grains. Astrophys J 1973;186:705–14.
[70] Goodman JJ, Draine BT, Flatau PJ. Application of fast-Fourier-transform techniques to the discrete-dipole approximation. Opt Lett 1991;16:1198–200.
[71] Draine BT, Goodman JJ. Beyond Clausius–Mossotti: wave propagation on a polarizable point lattice and the discrete dipole approximation. Astrophys J 1993;405:685–97.
[72] Penttilä A, Zubko E, Lumme K, Muinonen K, Yurkin MA, Draine B, et al. Comparison between discrete dipole implementations and exact techniques. JQSRT 2007;106:417–36.
[73] Hadamcik E, Levasseur-Regourd AC. Imaging polarimetry of cometary dust: different comets and phase angles. JQSRT 2003;79:661–78.
[74] Hadamcik E, Levasseur-Regourd AC. Dust evolution of comet C/1995 O1 (Hale-Bopp) by imaging polarimetric observations. Astron Astrophhys 2003;403:757–68.
[75] Mishchenko MI, Travis LD, Lacis AA. Multiple scattering of light by particles: radiative transfer and coherent backscattering. Cambridge, UK: Cambridge U. Press; 2006.
[76] Jessberger E. Rocky cometary particulates: their elemental, isotopic and mineralogical ingredients. Space Sci. Rev 1999;90:91–7.
[77] Jenniskens P. Optical constants of organic refractory residue. Astron Astrophys 1993;274:653–61.